Desalination and Water Treatment
www.deswater.com

doi: 10.5004/dwt.2020.25813

201 (2020) 43–54
October

The influence of nanosheets' size on pressure assisted self-assembly graphene oxide nanofiltration membrane

Yi Wei[a,b,c,*], Xueli Gao[a,b,*], Xiaojuan Wang[a,b], Baohua He[d], Congjie Gao[a,b]

[a]*Key Laboratory of Marine Chemistry Theory and Technology, Ministry of Education, Ocean University of China, No. 238, Songling Road, Qingdao 266100, China, Tel. +86 13012488897; email: weiyi@lzu.edu.cn (Y. Wei), Tel. +86 532 66782017; email: gxl_ouc@126.com (X. Gao), Tel. +86 0532-66782017; email: safiya0524@163.com (X. Wang), Tel. +86 0532-66782017; email: gaocj@zjut.edu.cn (C. Gao)*
[b]*College of Chemistry and Chemical Engineering, Ocean University of China, No. 238, Songling Road, Qingdao 266100, China*
[c]*Key Laboratory of Western China's Environmental System (Ministry of Education) and Gansu Engineering Research Center of Fine Particles Pollution Control Technology and Equipment, College of Earth and Environmental Science, Lanzhou University, No. 222, Tianshui South Road, Lanzhou 730000, China*
[d]*Gansu Membrane Science and Technology Research Insititute Co., Ltd., No. 1272, Duanjiatan, Lanzhou 730000, China, Tel. +86 13803205230; email: 331481677@qq.com (B. He)*

Received 25 July 2019; Accepted 7 March 2020

ABSTRACT

The size of graphene oxide (GO) has an effect on the properties of GO membranes (GOMs). However, the relationship between the influences of size and oxidation degree of GO on GOMs has not been thoroughly studied. In this study, we prepare to GO with different sizes by adjusting ultrasonic power and reduce GO in alkaline reduction. Pressure assisted self-assembly method is used to fabricate GO and reduced GOMs. The decreasing size increases the roughness and flux of GOM, and weakens the effect of reduction on the enhancement of the permeability of GOM. Even the permeability is reduced by reduction when the size is small enough. The penetration mechanism is related to the size of nanosheets that would influence the wrinkled structure, the wetting performance, and the channel structure of GOM.

Keywords: Graphene oxide; Nanosheets size; Nanofiltration membrane; Self-assembly; Desalination

1. Introduction

The technology of membrane desalination has been the main method to obtain sustainable fresh water from seawater or brackish water [1,2]. Many nanomaterials have been used for fabricating or modifying desalination membranes [3–6]. Because of the two-dimensional structure and negligible thickness, graphene-based materials have attracted a lot of attention in the water desalination and purification membrane [7–10]. The water permeability of single-layered nanoporous graphene is several orders higher than conventional reverse osmosis membranes [11]. As with most nanomaterials, graphene-based materials have also been used to modify conventional separation membranes [12–16]. As a derivative of graphene, graphene oxide (GO) has good dispersibility in water with the help of abundant oxygen-containing functional groups [17]. Based on the two-dimensional structure and hydrophilicity, GO has been widely applied in the separation membrane with a

* Corresponding authors.

multi-layered structure, by pressure-assisted self-assembly, spin self-assembly, or layer-by-layer self-assembly [18–27]. Water permeation routes in the multilayered GO membrane (GOM) can be divided into two parts: spaces under GO nanosheets and spaces between adjacent nanosheets [28]. Oxygen atoms in GO nanosheets are arranged in an orderly manner and some regions in GO nanosheets are nonoxidized [29,30]. Space between nonoxidized regions, which is larger than it in oxidized spaces and has relatively low frictional coefficient for water flowing [31–33], provides a network that allows the nearly frictionless flow of two or three layers of water molecules [34,35]. According to the different oxidized degrees of GO nanosheets, GOM has different layer spacing, which could be expanded in water [36,37]. Reduction of GO can increase the area of the nonoxidized region and the number of holes [38]. According to these mechanisms, researchers fabricated reduced graphene oxide (rGO) to facilitate water permeability of GOM [39–42]. Qiu et al. [39] used a hydrothermal method to prepare rGO, and found that reduced GOM (rGOM) had higher flux than GOM. Zhao et al. [40] also fabricated rGO by a simple hydrothermal reduction method and the flux promoted significantly when the reducing temperature was higher than 150°C. Shi et al. [42] prepared GOM with a tunable structure by controlling the oxidation degree of GO. In spite of poor hydrophilicity, rGOM, with the more nonoxidized region and wrinkled structure, showed higher flux. These results verified the mechanism that water molecules in the nonoxidized region had low friction resistance and reduction could disrupt the layered structure. Except for tuning the oxidation degree, the functionalization of GO is also an effective way to regulate membrane properties [43,44]. The physical and chemical properties of GO mainly include oxidation degree, oxygenated functional groups, and size of nanosheets. Cohen-Tanugi et al. [45] used a bilayer nanoporous graphene membrane to investigate the influence of nanoporous offset, which was related to the size of nanosheets. This research indicated that the water flowrate was almost independent of the pore offset, but the salt rejection increased with bigger nanoporous offset when the radius of nanopores was 4.5 Å. Sun et al. [46] found that the permeation rate of ions through GOM made from nanosized sheets was faster than that from microsized sheets under forward osmosis mode. However, the influence of nanosheets' size on the performance of GOM and rGOM, including flux and rejection under pressure-driven mode, has not been studied in detail.

In this work, we fabricated GO with different sizes and reduced them in alkali conditions. The size of GO was controlled by adjusting the ultrasonic power and characterized by atomic force microscopy (AFM). GO and rGO with different sizes were used to prepare membranes by pressure-assisted self-assembly method. All membranes were tested in a cross-flow pressurized membrane system. The results showed that GOM made of smaller nanosheets had lower penetration resistance and rGOM had higher flux than GOM when the size of nanosheets was hundreds of nanometers. However, when the size was only tens of nanometers, rGOM had worse permeability than GOM. The influence of nanosheets' size on the performance of GOM and rGOM was explained and the penetration mechanism of GOMs was discussed.

2. Experimental

2.1. Synthesis and characterization of GO and rGO

Modified Hummers method was used to fabricate GO [47]. Firstly, expandable graphite (99%, Qingdao Laixi Nanshu Fada Graphite Co.) was added into a mixture of concentrated H_2SO_4 (95 wt.%, Beijing Chemical Works) and $KMnO_4$ (99%, Sinopharm Chemical Reagent Co., Ltd.) below 5°C and stirred for 30 min. Secondly, the mixture was heated to 35°C for 2.5 h. Thirdly, the resulting mixture was diluted and heated up to 95°C for 15 min. A large amount of DI water was then added into the mixture to terminate the reaction. After natural cooling, hydrogen peroxide (30%, Tianjin Basf Co., Ltd.) was added and the color of suspension liquid changed from brown to golden yellow. Finally, graphite oxide was obtained by washing with HCl (10%, Beijing Chemical Works) and DI water for several times until the pH value was stable. Graphite oxide was vacuum-dried under 40°C. GO solutions were prepared by using ultrasonic exfoliation (in ultrasonic cell grinder,48.75 W, 80 min) and centrifugation (8,000 rpm, 10 min). As seen in Table 1, GO with a smaller size was fabricated by additional ultrasonic crushing in ultrasonic cell grinder with different ultrasonic power. To prepare rGO, a certain amount of NaOH (98%, Beijing Chemical Works) solution was added into GO solution until the pH value was 12. The alkaline solution was stirred for 24 h at home temperature and neutralized by adding HCl. NaCl in rGO solution was removed by dialyzing for over 48 h.

GO and rGO were characterized by Fourier transform infrared spectroscopy (FTIR, Bruker Tensor 27), X-ray photoelectron spectroscopy (XPS, Thermo Fisher SCIENTIFIC ESCALAB 250), and AFM (Veeco Multimode-V microscope). The FTIR was performed by using pressed KBr flakes at room temperature. The XPS was measured on the film surface with an achromatic X-ray source of 100 W and 15 kv. The AFM samples were obtained by dropping GO or rGO solution on mica slice and tested under tapping mode.

2.2. Synthesis and characterization of GOM and rGOM

The progress of the preparation of GOM or rGOM was illustrated in our previous study [48]. A self-designed membrane cell, which could hold 100 mL of GO/rGO solution, was used to prepare GOM/rGOM by dead-end filtration. The GO or rGO solution (100 mL), with a concentration of 0.01 mg mL^{-1}, was filtrated at 0.2 MPa through UF membranes (details in ESI) with a diameter of 7.5 cm. The pressure was maintained until there was no obvious water on the surface of GOM or rGOM. Finally, the wet GOM or rGOM was dried in vacuo at 40°C for at least 24 h.

Table 1
Ultrasonic parameters of exfoliation and crushing process for different size of GO or rGO

	GO1/rGO1	GO2/rGO2	GO3/rGO3
Exfoliation	48.75 W, 80 min	48.75 W, 80 min	48.75 W, 80 min
Crushing	None	162.5 W, 40 min	325 W, 40 min

The surface morphology of GOM and rGOM were obtained by scanning electron microscope (SEM, Hitachi S-4800) and AFM. Gold sputtering was done on SEM samples. The hydrophilicity of the membrane was characterized by a contact angle (CA) analyzer (Kruss DSA100). All samples were dried before measurement. The CA data were recorded for 120 s. The penetration and separation performances of membranes were tested using a nanofiltration membrane performance evaluation instrument (Hangzhou Yueliangquan Co., Ltd.). Ahead of measurement, all samples were pre-pressured at 2.0 MPa for at least 2 h to ensure membrane compaction. The salt concentration was measured by a digital conductivity instrument (DDS-307A, Leici, China). The layer spacing was measured by X-ray diffraction (XRD, D8 ADBANCE), which was equipped with a Cu Kα radiation at the rate of 1°min^{-1}, to reveal the interlayer spacing of GO and rGO.

The *d*-spacing of GO or rGO can be calculated via Braggs law:

$$\lambda = 2d\sin\theta \tag{1}$$

where λ is the wavelength of the X-ray, d is the interlayer spacing, θ means the diffraction angle.

The water flux and salt rejection were calculated according to the following equations:

$$F = \frac{V}{A \cdot \Delta t} \tag{2}$$

where F is the flux of membranes (L m^{-2} h^{-1}), V is the permeate volume (L), A is the effective membrane area (m^2), Δt is the time to collect product water (h).

$$R(\%) = \left(1 - \frac{C_p}{C_f}\right) \times 100 \tag{3}$$

where R means the rejection of membranes (%), C_f and C_p are the concentration in the feed and permeate solution, respectively.

3. Result and discussion

3.1. AFM images of GO with different size

To investigate the size of GO nanosheets, AFM images are carried out. Fig. 1 shows AFM images of GO1, GO2, and GO3. GO in Fig. 1a was exfoliated in water with ultrasonic power of 48.75 W and the biggest size is more than 500 nm. After additional ultrasonic crushing, GO nanosheets were cut into smaller pieces. The maximum size of GO2 nanosheets is about 200 nm in Fig. 1b. As seen in Fig. 1c, nanosheets are smaller and the size is about dozens of nanometers.

3.2. FTIR spectroscopy of GO and rGO

The oxygen-containing groups in GO and rGO were confirmed by FTIR spectroscopy, which is consistent with published papers [49,50]. As shown in Fig. 2, the intensities of the peaks corresponding to oxygen-containing functional groups, such as the C=O stretching vibration peak at 1,727 cm^{-1}, the C–O (epoxy) stretching vibration peak at 1,227 cm^{-1}, and the C–O (alkoxy) stretching vibration peak at 1,045 cm^{-1} decrease obviously. The intensities of peaks at 1,227 and 1,045 cm^{-1} is significantly reduced. This result indicates that alkaline reduction has a stronger effect on C–O than C=O. The peak at 1,727 cm^{-1} in the rGO spectrum became weaker but still clear, indicating that the reduction of C=O is not very drastic. Shen et al. [51] also found that the reduction of epoxy and hydroxyl groups were more sharply than carbonyl and carboxyl groups [51].

3.3. XPS spectroscopy of GO and rGO

The reduction of GO was also characterized by using XPS. Fig. 3 shows the $C1_s$ XPS spectra of GO and rGO. The peaks 1, 2, 3, and 4 correspond to C=C/C–C (aromatic rings), C–O (epoxy and alkoxy), C=O, and COOH groups, respectively. After reduction by NaOH, the ratio of carbon to oxygen increases from 67/33 to 69/31. According to the peak result, the intensity of peak 2 (C–O) weakened significantly. Calculation result of peak area is shown in Table 2. Compared with peak 1 (C=C/C–C), the relative area ratio

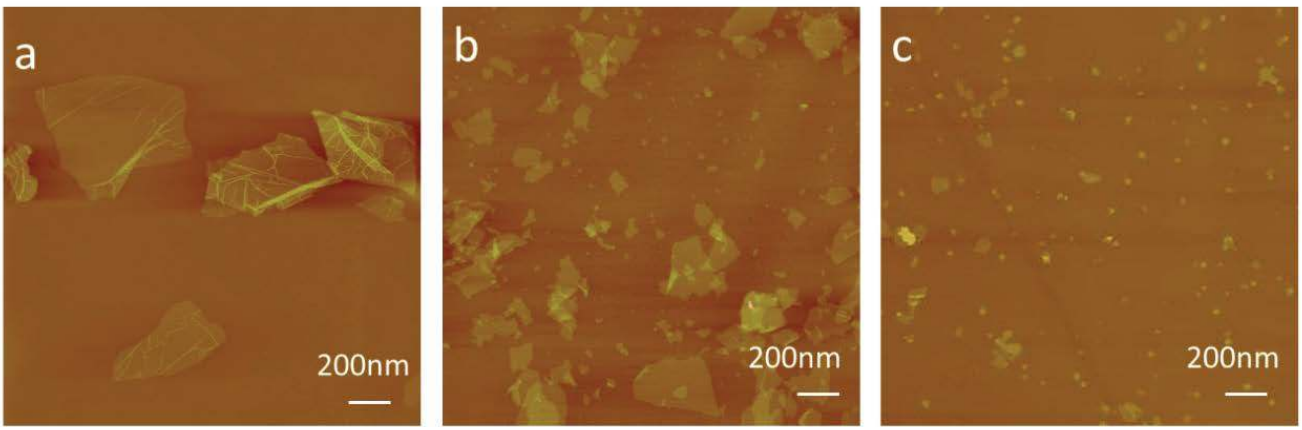

Fig. 1. AFM images of GO nanosheets with different ultrasonic power (a) GO1, (b) GO2, and (c) GO3.

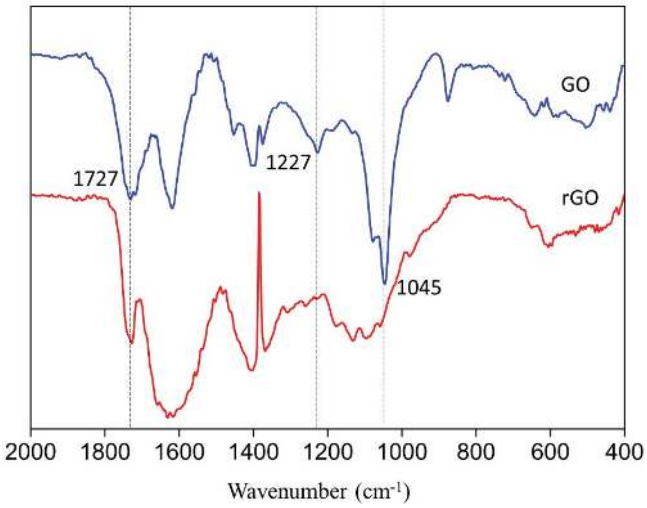

Fig. 2. FTIR spectra of GO and rGO.

of peak 2 (C–O) decreases from 116% to 96%. Peak 3 (C=O) and peak 4 (COOH) also become weaker. The XPS results, consistent with the FTIR results, reveal that some oxygen-containing functional groups in the plane and on the edge are removed after reduction.

3.4. XRD spectroscopy of GO and rGO

XRD patterns of GO and rGO are illustrated in Fig. 4. The three diffraction peaks presenting at 17.8°, 22.7°, and 26.0° correspond to the ultrafiltration membrane [48]. According to previous research, the layer spacing of GO is influenced by the oxidation degree. By using the Bragg formula to calculate the XRD results (Fig. 4), we found that the layer spacing of rGOM (0.82 nm) is narrower than GOM (0.86 nm). The height profiles of AFM images are also illustrated in Fig. 5. The thickness of GO nanosheet is 0.692 nm, which is thicker than that of rGO nanosheet.

3.5. Visual observation of GO and rGO

The GO and rGO solutions with different size were filtered and deposited on UF membranes. Visual observation

Table 2
Peaks area of XPS C1s spectra in Fig. 3

	Peak 1	Peak 2	Peak 3	Peak 4
GO	100%	116%	15%	8%
rGO	100%	96%	11%	6%

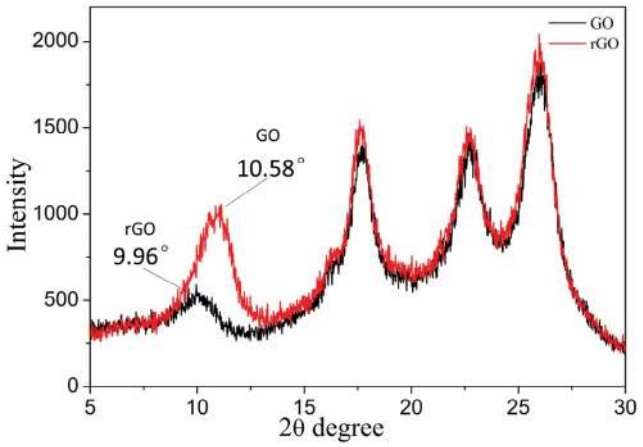

Fig. 4. XRD spectra of GO and rGO membranes.

is a simple way to see the difference between GO and rGO. Fig. 6 shows the digital photos of GO and rGO. Obviously, the color of rGO is deeper than GO.

3.6. Morphology of GOM and rGOM

Morphological structure of GOM and rGOM was characterized by using SEM and AFM. SEM surface images of GOM and rGOM are provided in Fig. 7. Most areas of GOMs are flat and there is no obvious difference in three kinds of GOM. Additionally, it can be seen clearly that the reduction of GO can increase the number of wrinkles. Wrinkles on GOM or rGOM are formed from the initial corrugation of nanosheets [52,53]. The corrugation can be enhanced by the decomposition of the oxygen functional

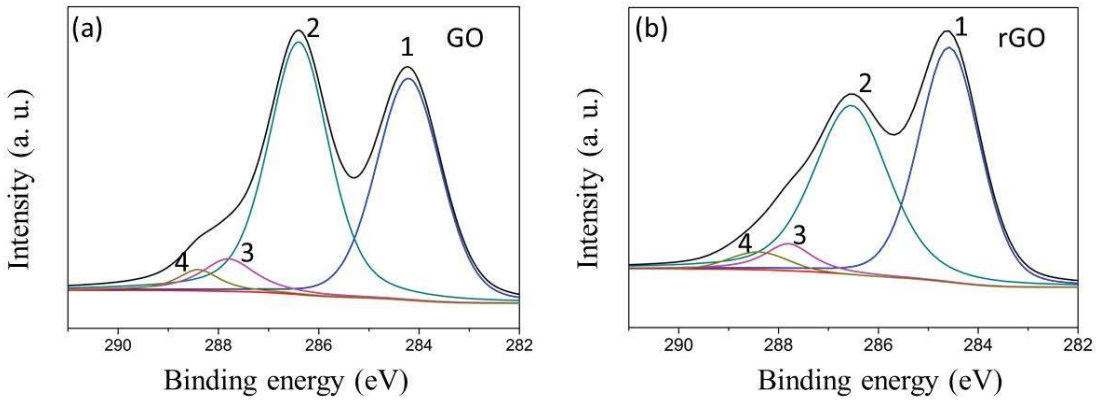

Fig. 3. XPS C1s spectra of GO (a) and rGO (b). Peaks 1–4 correspond to (C=C/C–C), (C–O), (C=O), and (COOH), respectively.

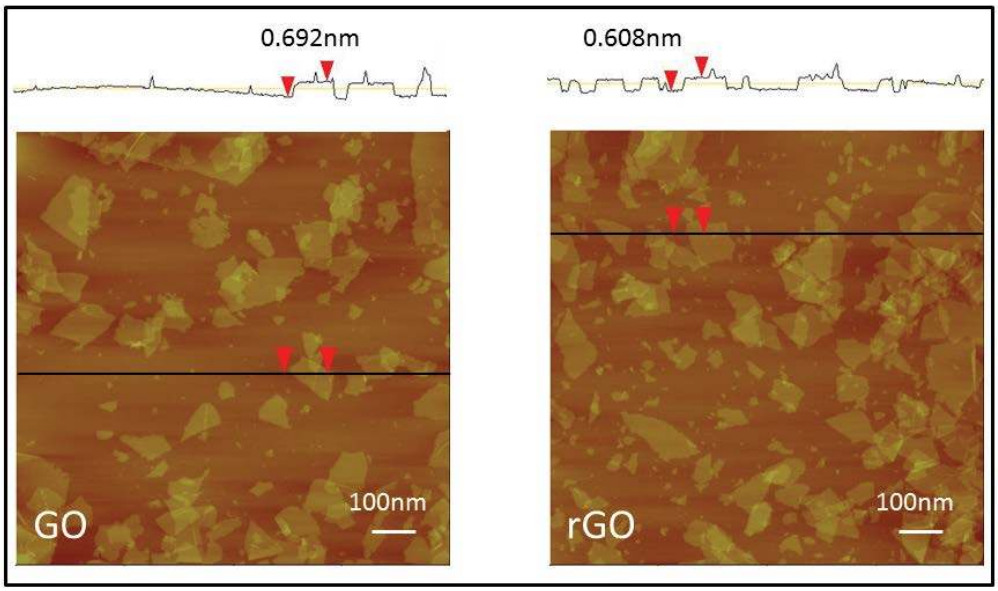

Fig. 5. AFM images and Height profiles of GO and rGO nanosheets.

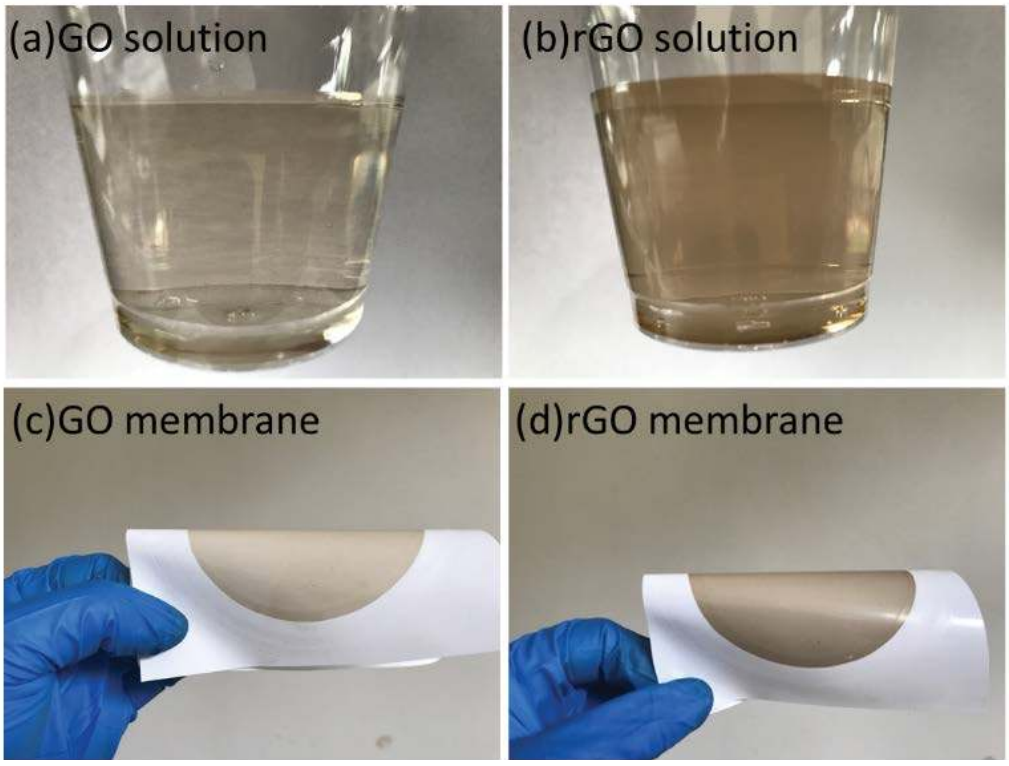

Fig. 6. Digital photos of GO solution (a), rGO solution (b), GOM (c), and rGOM (d).

groups [54]. Zhao et al. [40] also found that the flatness of reduced GO nanosheets was worse than GO nanosheets.

To get more detailed morphological information, the flat areas in SEM images were characterized by AFM. According to Fig. 8, there is no obvious difference between GO1M and GO2M membrane. However, in Fig. 8c1, wrinkles were much more than Fig. 8a1 and b1. The roughness values are also illustrated in Fig. 8. RMS value is the root mean square roughness and Ra value is the average roughness. Although GO1M and GO2M have almost the same surface topography by visual look, the roughness values of GO2M is higher than GO1M. In our previous study, we had illustrated the formation of wrinkles on GOMs and their influence on separation performance [48]. As seen in Fig. 1, the size of GO3 is the smallest in three samples. In the self-assembly process, initial wrinkles, folding of GO,

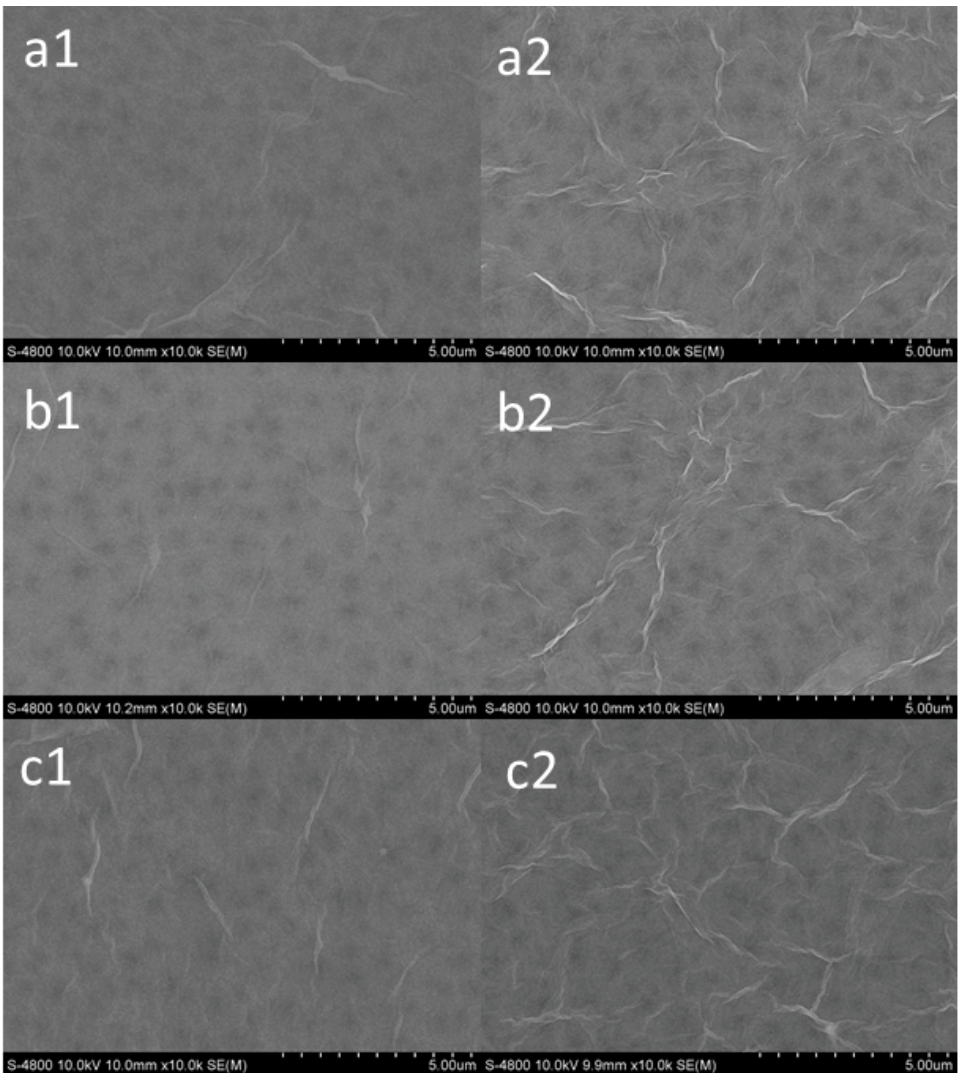

Fig. 7. SEM images of GOM and rGOM (a1) GO1M, (b1) GO2M, (c1) GO3M, (a2) rGO1M, (b2) rGO2M, and (c2) rGO3M.

and stacking of GO can develop into wrinkles on the surface as seen in AFM and SEM images. Lin et al. [55] found that the edge-to-edge interactions of GO nanosheets also played a key role in determining the wrinkled structure and larger GO nanosheets containing fewer edge-to-edge interactions possessed a less-wrinkled structure. At the same mass concentration, GO3 has a smaller size and more nanosheets. Lots of edge-to-edge interaction results in more initial wrinkles which can lead to more surface wrinkles. So, the RMS values increase with the decreasing size of nanosheets. The RMS roughness of GO1M is 11.784 nm, in comparison, the roughness is increased to 14.992 nm after reduction. GO2M has the same change of roughness after reduction. The increased roughness of rGO1M and rGO2M is associated to increased wrinkles, because reduction will cause more initial wrinkles [38]. However, compared with GO3M or rGO2M, the roughness of rGO3M is smaller. There are two main reasons for this phenomenon. Firstly, gentler wrinkles, which can be seen in Fig. 8c2, will result in a lower roughness value. Secondly, smaller nanosheets size will lead to more initial wrinkles. When the initial wrinkles are closer, as the nanosheets are deposited, many initial wrinkles may not develop into surface wrinkles. This is similar to the bridging effect. The adjacent initial wrinkles are piers, and a relatively flat bridge surface is formed between them. So, when the size of the rGO nanosheets is small enough, the value of surface roughness will decrease.

3.7. Hydrophilicity and wetting performance of GOM and rGOM

The contact angle was measured at room temperature with indoor humidity of 50% ± 5%. The hydrophilicity of the membrane was evaluated by measuring the CA of droplet after contact with the membrane for three seconds. The wetting performance of the membrane was characterized by recording the change of CA in 120 s. As displayed in Fig. 9, the CA of rGOM is higher than GOM. The increasing of CA implies that the reduction makes rGOM more hydrophobic than GOM. Additionally, because of the more wrinkled surface, the CA of GOM and rGOM decrease with

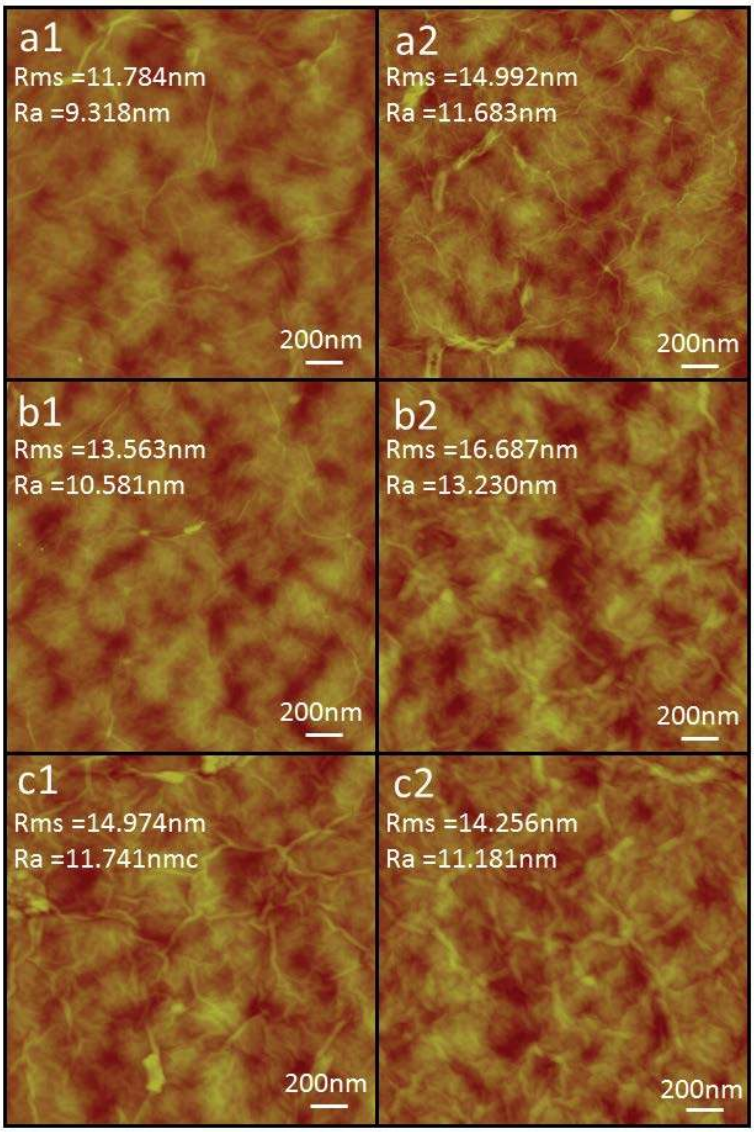

Fig. 8. AFM images of GOM and rGOM (a1) GO1M, (b1) GO2M, (c1) GO3M, (a2) rGO1M, (b2) rGO2M, and (c2) rGO3M.

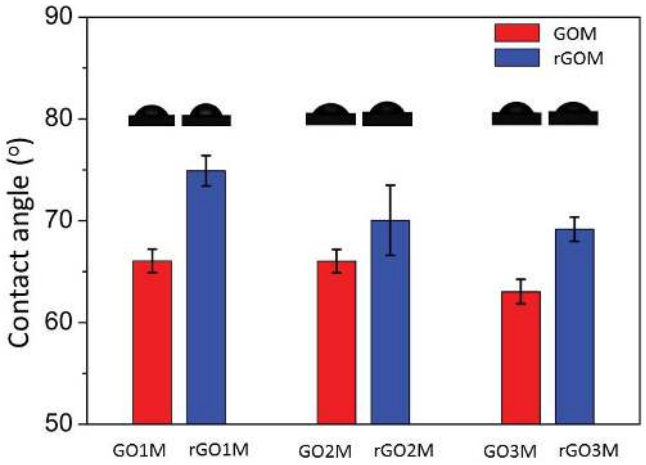

Fig. 9. Water contact angle of GOM and rGOM.

decreasing the size of nanosheets. Increased roughness helps increase the hydrophilicity or hydrophobicity of the surface as shown by CA [56], because the macro gully is more conducive to the spread of water. In addition, GO3M or rGO3M has more gaps on the surface, which allow water to enter the membrane quickly. GO or rGO nanosheets will be more hydrophilic when exposed to water.

The size of GO/rGO nanosheets can also affect the wetting performance of the membrane. As shown in Fig. 10, the speed of contact angle reduction increases with the decreasing size of nanosheets. Because wet GOM is more hydrophilic than dry GO, the attenuation of CA is due to the infiltration of water into the membrane. In the process of contact angle testing, water molecules enter into the gaps and diffuse in the layer spacing driven by capillary force. There are many gaps between adjacent nanosheets on the surface of GOM. As an entrance of the water channel, the gap is one of the important factors affecting the

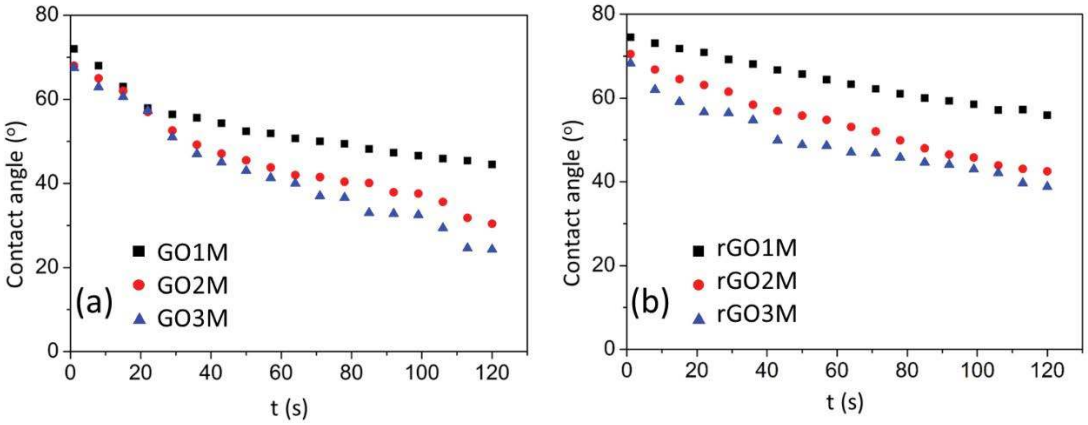

Fig. 10. Water contact angle reduction of GOM (a) and rGOM (b) with time.

permeability of the membrane. The number of gaps is influenced by the size of nanosheets. With the decreasing size of GO nanosheets, there are more gaps on the surface of GOM, and water molecules have more entrances to enter into the membrane. Compared between GOM (Fig. 10a) and rGOM (Fig. 10b), the reduction of GO can decrease the infiltration rate of water into membranes. The reduction decreases the layer spacing (Fig. 4) and the number of oxygen-containing functional groups (Fig. 3). Reduced oxygen-containing functional groups lead to poorer surface hydrophilicity and smaller layer spacing results in higher osmosis resistance. Although we mentioned in the section introduction that some studies found that reduction of GO can increase the area of the nonoxidized region and holes to achieve higher permeability, the osmosis of water during the measurement of CA was different from the movement of water caused by hydraulic pressure. Here, the osmosis of water into GO/rGOM refers to the hydrophilicity of oxygen-containing functional groups and wide water channel. Nonoxidized region with low friction resistance facilitates water movement under pressure.

3.8. Separation performance of GOM and rGOM

According to Fig. 11, the flux of GOM increases with the decreasing size of nanosheets. At the same GO concentration, the flux of GO3M is about twice that of GO1M. This phenomenon can be explained in three reasons. Firstly, as explained before, GO3M has more gaps on the surface because of smaller nanosheets. Water molecules on the membrane surface have more entrances to flow into water channels. Secondly, the smaller size of nanosheets means a shorter channel in which water molecules transport through the whole membrane. As seen in Fig. 12, water molecules enter into the gaps between adjacent nanosheets or holes and move in the first layer spacing. When moving to the next gap or hole, water molecules enter into the next layer spacing. Like this, water molecules pass through the entire membrane. If the size of nanosheets is smaller, the length of the water channel would be shorter and water molecules can transport through the membrane more quickly. Muscatello et al. [57] found that the

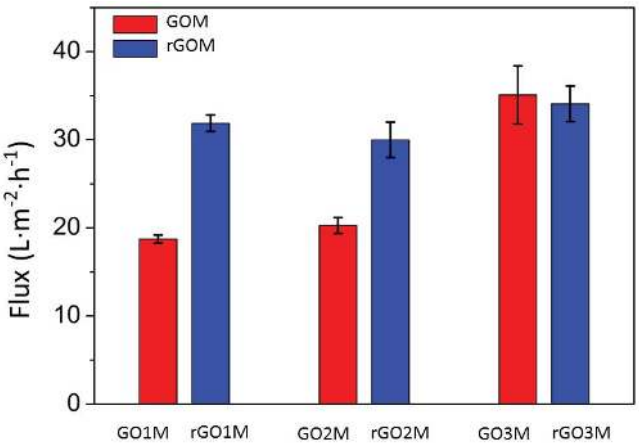

Fig. 11. Pure water fluxes of GOM and rGOM.

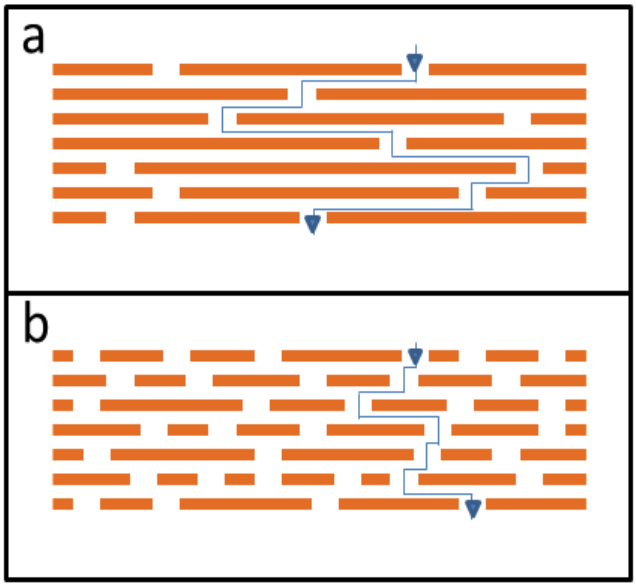

Fig. 12. Schematic diagram of channel length in GOM made by large nanosheets (a) and small nanosheets (b).

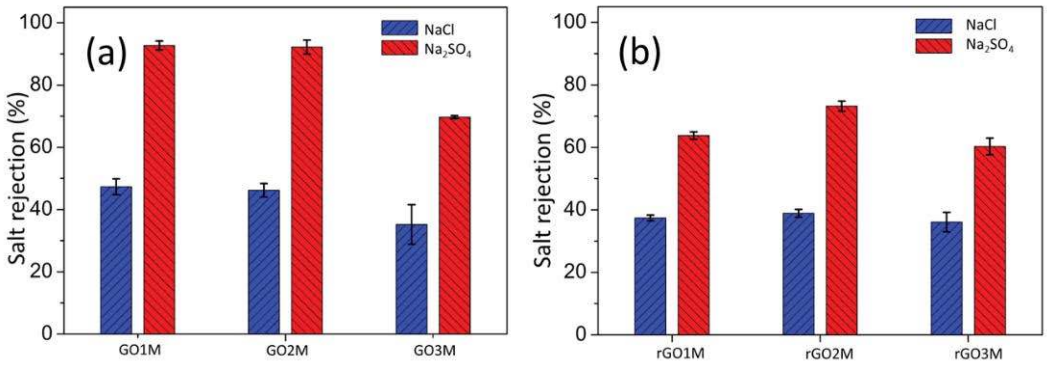

Fig. 13. Salt rejection of GOM (a) and rGOM (b)

permeability depended on the length of the path taken by water molecules. Thirdly, as seen in Fig. 8, the number of wrinkles increases with the decreasing size of nanosheets. These wrinkles could provide water channels with larger size [18,19]. The water channel under wrinkles are larger than it under the flat area, thus has lower resistance for water permeation. A more wrinkled structure means lower penetration resistance. Based on the above three reasons, GO3M has the highest flux at the same mass concentration.

After alkaline reduction, the flux of rGO1M is higher than GO1M obviously. Qiu et al. [39] found that the flux increased with increasing temperature of hydrothermal treatment. The flux of 150°C-membrane is five times higher than 90°C-membrane. Another group also published that hydrothermal reduction could increase the flux of GOM [40]. In our experiments, the size of GO nanosheets can influence the effect of reduction on membrane flux. As seen in Fig. 11, the flux of rGO2M is also higher than GO2M, but the degree of flux change is significantly less than between rGO1M and GO1M. Especially, the permeability of rGO3M is worse than GO3M. The higher fluxes of rGO1M and rGO2M are associated to the increased nonoxidized area of GO nanosheets and a more-wrinkled structure of the membrane. After reduction, some oxidized region on GO is converted to nonoxidized region with a smoother surface, larger space, and lower flow resistance [28,33,58]. Additionally, as seen in Figs. 7 and 8, rGO1M and rGO2M have more wrinkles than GO1M and GO2M, respectively. The wrinkle provides more channels with low resistance. The roughness value also reflects this phenomenon. Therefore, rGO1M and rGO2M have lower penetration resistance than GO1M and GO2M, respectively. However, from GO3M to rGO3M, average flux is decreased. After high-intensity ultrasonic crushing, the size of GO nanosheets decreases. As seen in Fig. 12, the water channel is made up of vertical and horizontal parts. Nonoxidized region is an important part of the horizontal channel. With the decrease of nanosheets size, the horizontal part of the channel reduces gradually. Decreased size of nanosheets reduces the contribution of the nonoxidized region to permeability, although reduction can increase the area of the nonoxidized region. On the other hand, the AFM image (Fig. 8) reveals that GO3M and rGO3M have almost the same surface morphology. The less hydrophilic surface may be the only way to explain the decreased flux from GO3M to rGO3M.

The salt rejection (R) is also an important parameter to reflect the filtration performance of GOM and rGOM. According to the Donnan exclusion theory, which is usually used to explain the separation mechanism of the nanofiltration membrane [59,60], negatively charged GOM has higher retention for the bivalent anion. After reduction, the penetration resistance of rGO1M or rGO2M decreases obviously so that R (NaCl) and R (Na_2SO_4) decrease simultaneously. For rGO1M, its salt rejection is lower than GO1M (Fig. 13). R (NaCl) and R ($Na_2SO_{4)}$ decrease from 47.3% and 92.7% to 37.4% and 63.8%, respectively. The decline in R (rGO2M) is smaller than R (rGO1M) and the flux change of rGO2M is also smaller than rGO1M. It is obvious that the effect of reduction on rGO2M is weaker than it on rGO1M. For GO3M and rGO3M, R (NaCl) is almost the same, and R (Na_2SO_4) decreases from 69.7% to 60.3%. The retention for salt is contributed by size-exclusion effect and electrostatic interaction. As the sulfate is a divalent anion, the retention for Na_2SO_4 is more dependent on the electrostatic interaction effect. The loss of oxygen-containing functional groups caused by reduction reduces the effect of electrostatic interaction. The rejection of NaCl is more dependent on the size-exclusion effect. According to Fig. 11, the difference in flux between rGO3M and GO3M is very small, indicating that their penetration resistance is almost constant. The electrostatic repulsion effect becomes weaker after reduction and the penetration resistance could remain unchanged when the size of the nanosheet is small enough.

4. Conclusion

We prepared GO nanosheets with different sizes by ultrasonic crushing under different power. High-power ultrasound can crush nanosheets. We used three different sizes of GO nanosheets to fabricate GOM by pressure-assisted self-assembly method. The flux of GOM is increased with the decreasing size of nanosheets. The surface topography and wetting performance are significantly affected by the size of nanosheets. To investigate the penetration mechanism more thoroughly, we reduced GO in an alkaline environment to increase the area of the nonoxidized region. The flux of rGOM made of large nanosheets is higher than GOM. Decreased size of nanosheets can reduce the flux difference between GOM and rGOM and even make rGOM having lower permeability than GOM. The permeability

of GOM can be influenced by the size of GO nanosheets. Furthermore, decreasing the size of nanosheets can reduce the effect of oxidation on separation performance. The effect of nanosheets' size should be taken into account when explaining the permeation mechanism of GOM.

Acknowledgments

Funding for this study was provided by the National Key Research and Development Projects (No. 2017YFC0403901), the National Natural Science Foundation of China (No. 21576250), Major Science and Technology Projects of Gansu (No. 17ZD2WA002), the Young Taishan Scholars Program of Shandong Province, and the Fundamental Research Funds for the Central Universities.

Appendix A: Supplementary data

Supplementary data to this article can be found online.

References

[1] M. Elimelech, W.A. Phillip, The future of seawater desalination: energy, technology, and the environment, Science, 333 (2011) 712–717.
[2] G.M. Geise, H.S. Lee, D.J. Miller, B.D. Freeman, J.E. McGrath, D.R. Paul, Water purification by membranes: the role of polymer science, J. Polym. Sci., Part B: Polym. Phys., 48 (2010) 1685–1718.
[3] H. Zhao, Q. Shi, L. Wu, L. Zhang, H. Chen, C. Gao, Improving the performance of polyamide reverse osmosis membrane by incorporation of modified multi-walled carbon nanotubes, J. Membr. Sci., 450 (2014) 249–256.
[4] M.E. Suk, A.V. Raghunathan, N.R. Aluru, Fast reverse osmosis using boron nitride and carbon nanotubes, Appl. Phys. Lett., 92 (2008), doi: 10.1063/1.2907333.
[5] W. Choi, J. Choi, J. Bang, J.H. Lee, Layer-by-layer assembly of graphene oxide nanosheets on polyamide membranes for durable reverse-osmosis applications, ACS Appl. Mater. Interfaces, 5 (2013) 12510–12519.
[6] J. Duan, Y. Pan, F. Pacheco, E. Litwiller, Z. Lai, I. Pinnau, High-performance polyamide thin-film-nanocomposite reverse osmosis membranes containing hydrophobic zeolitic imidazolate framework-8, J. Membr. Sci., 476 (2015) 303–310.
[7] D. Cohen-Tanugi, J.C. Grossman, Nanoporous graphene as a reverse osmosis membrane: recent insights from theory and simulation, Desalination, 366 (2015) 59–70.
[8] K.A. Mahmoud, B. Mansoor, A. Mansour, M. Khraisheh, Functional graphene nanosheets: the next generation membranes for water desalination, Desalination, 356 (2015) 208–225.
[9] R.K. Joshi, S. Alwarappan, M. Yoshimura, V. Sahajwalla, Y. Nishina, Graphene oxide: the new membrane material, Appl. Mater. Today, 1 (2015) 1–12.
[10] L. Huang, M. Zhang, C. Li, G. Shi, Graphene-based membranes for molecular separation, J. Phys. Chem. Lett., 6 (2015) 2806–2815.
[11] D. Cohen-Tanugi, J.C. Grossman, Water desalination across nanoporous graphene, Nano Lett., 12 (2012) 3602–3608.
[12] S. Zinadini, A.A. Zinatizadeh, M. Rahimi, V. Vatanpour, H. Zangeneh, Preparation of a novel antifouling mixed matrix PES membrane by embedding graphene oxide nanoplates, J. Membr. Sci., 453 (2014) 292–301.
[13] J. Wang, X. Gao, J. Wang, Y. Wei, Z. Li, C. Gao, O-(carboxymethyl)-chitosan nanofiltration membrane surface functionalized with graphene oxide nanosheets for enhanced desalting properties, ACS Appl. Mater. Interfaces, 7 (2015) 4381–4389.
[14] H. Chae, J. Lee, C. Lee, I. Kim, P. Park, Graphene oxide-embedded thin-film composite reverse osmosis membrane with high flux, anti-biofouling, and chlorine resistance, J. Membr. Sci., 483 (2015) 128–135.
[15] L. Shen, S. Xiong, Y. Wang, Graphene oxide incorporated thin-film composite membranes for forward osmosis applications, Chem. Eng. Sci., 143 (2016) 194–205.
[16] M.E.A. Ali, L. Wang, X. Wang, X. Feng, Thin film composite membranes embedded with graphene oxide for water desalination, Desalination, 386 (2016) 67–76.
[17] Y. Si, E.T. Samulski, Synthesis of water soluble graphene, Nano Lett., 8 (2008) 1679–1682.
[18] H. Huang, Y. Mao, Y. Ying, Y. Liu, L. Sun, X. Peng, Salt concentration, pH and pressure controlled separation of small molecules through lamellar graphene oxide membranes, Chem. Commun., 49 (2013) 5963–5965.
[19] H. Huang, Z. Song, N. Wei, L. Shi, Y. Mao, Y. Ying, L. Sun, Z. Xu, X. Peng, Ultrafast viscous water flow through nanostrand-channelled graphene oxide membranes, Nat. Commun., 4 (2013) 2979–2987.
[20] Y. Han, Z. Xu, C. Gao, Ultrathin graphene nanofiltration membrane for water purification, Adv. Funct. Mater., 23 (2013) 3693–3700.
[21] R.R. Nair, H.A. Wu, P.N. Jayaram, I.V. Grigorieva, A.K. Geim, Unimpeded permeation of water through helium-leak − tight graphene-based membranes, Science, 335 (2012) 442–444.
[22] R.K. Joshi, P. Carbone, F.C. Wang, V.G. Kravets, Y. Su, I.V. Grigorieva, H.A. Wu, A.K. Geim, R.R. Nair, Precise and ultrafast molecular sieving through graphene oxide membranes, Science, 343 (2014) 752–754.
[23] L. Wang, N. Wang, J. Li, J. Li, W. Bian, S. Ji, Layer-by-layer self-assembly of polycation/GO nanofiltration membrane with enhanced stability and fouling resistance, Sep. Purif. Technol., 160 (2016) 123–131.
[24] Y. Zhang, S. Zhang, J. Gao, T. Chung, Layer-by-layer construction of graphene oxide (GO) framework composite membranes for highly efficient heavy metal removal, J. Membr. Sci., 515 (2016) 230–237.
[25] M. Hu, B. Mi, Layer-by-layer assembly of graphene oxide membranes via electrostatic interaction, J. Membr., Sci., 469 (2014) 80–87.
[26] K. Huang, G. Liu, Y. Lou, Z. Dong, J. Shen, W. Jin, A graphene oxide membrane with highly selective molecular separation of aqueous organic solution, Angew. Chem. Int. Ed., 53 (2014) 6929–6932.
[27] K.H. Lee, J.H. Hong, S.J. Kwak, P. Min, J.G. Son, Spin self-assembly of highly ordered multilayers of graphene-oxide sheets for improving oxygen barrier performance of polyolefin films, Carbon, 83 (2015) 40–47.
[28] N. Wei, X. Peng, Z. Xu, Understanding water permeation in graphene oxide membranes, ACS Appl. Mater. Interfaces, 6 (2014) 5877–5883.
[29] D. Pacilé, J.C. Meyer, A. Fraile Rodríguez, M. Papagno, C. Gómez-Navarro, R.S. Sundaram, M. Burghard, K. Kern, C. Carbone, U. Kaiser, Electronic properties and atomic structure of graphene oxide membranes, Carbon, 49 (2011) 966–972.
[30] N.R. Wilson, P.A. Pandey, R. Beanland, R.J. Young, I.A. Kinloch, L. Gong, Z. Liu, K. Suenaga, J.P. Rourke, S.J. York, J. Sloan, Graphene oxide: structural analysis and application as a highly transparent support for electron microscopy, ACS Nano, 3 (2009) 2547–2556.
[31] R. Devanathan, D. Chasewoods, Y. Shin, D.W. Gotthold, Molecular dynamics simulations reveal that water diffusion between graphene oxide layers is slow, Sci. Rep., 6 (2016) 29484.
[32] J.A.L. Willcox, H.J. Kim, Molecular dynamics study of water flow across multiple layers of pristine, oxidized, and mixed regions of graphene oxide, ACS Nano, 11 (2017) 2187–2193.
[33] H. Dai, Z. Xu, X. Yang, Water permeation and ion rejection in layer-by-layer stacked graphene oxide nanochannels: a molecular dynamics simulation, J. Phys. Chem. C, 120 (2016) 22585–22596.
[34] D.W. Boukhvalov, M.I. Katsnelson, Y. Son, Origin of anomalous water permeation through graphene oxide membrane, Nano Lett., 13 (2013) 3930–3935.
[35] X. Peng, Z. Xu, N. Wei, Breakdown of fast water transport in graphene oxides, Phys. Rev. E, 89 (2014), doi: 10.1103/PhysRevE.89.012113

[36] W. Choi, K. Chun, J. Kim, C. Han, Ion transport through thermally reduced and mechanically stretched graphene oxide membrane, Carbon, 114 (2017) 377–382.
[37] A. Lerf, A. Buchsteiner, J. Pieper, S. Schöttl, I. Dekany, T. Szabo, H.P. Boehm, Hydration behavior and dynamics of water molecules in graphite oxide, J. Phys. Chem. Solids, 67 (2006) 1106–1110.
[38] K. Erickson, R. Erni, Z. Lee, N. Alem, W. Gannett, A. Zettl, Determination of the local chemical structure of graphene oxide and reduced graphene oxide, Adv. Mater., 22 (2010) 4467.
[39] L. Qiu, X. Zhang, W. Yang, Y. Wang, G.P. Simon, D. Li, Controllable corrugation of chemically converted graphene sheets in water and potential application for nanofiltration, Chem. Commun., 47 (2011) 5810–5812.
[40] Y. Zhao, C. Li, X. Fan, J. Wang, G. Yuan, X. Song, J. Chen, Z. Li, Study on the separation performance of the multi-channel reduced graphene oxide membranes, Appl. Surf. Sci., 384 (2016) 279–286.
[41] J. Zhu, L. Zhu, Z. Lu, L. Gu, S. Cao, X. Cao, Selectively expanding graphene oxide paper for creating multifunctional carbon materials, J. Phys. Chem. C, 116 (2012) 23075–23082.
[42] G. Shi, Q. Meng, Z. Zhao, H. Kuan, A. Michelmore, J. Ma, Facile fabrication of graphene membranes with readily tunable structures, ACS Appl. Mater. Interfaces, 7 (2015) 13745–13757.
[43] Y. Yuan, X. Gao, Y. Wei, X. Wang, J. Wang, Y. Zhang, C. Gao, Enhanced desalination performance of carboxyl functionalized graphene oxide nanofiltration membranes, Desalination, 405 (2017) 29–39.
[44] P. Sun, H. Liu, K. Wang, M. Zhong, D. Wu, H. Zhu, Selective ion transport through functionalized graphene membranes based on delicate ion–graphene interactions, J. Phys. Chem. C, 118 (2014) 19396–19401.
[45] D. Cohen-Tanugi, L. Lin, J.C. Grossman, Multilayer nanoporous graphene membranes for water desalination, Nano Lett., 16 (2016) 1027–1033.
[46] P. Sun, F. Zheng, M. Zhu, Z. Song, K. Wang, M. Zhong, D. Wu, R.B. Little, Z. Xu, H. Zhu, Selective trans-membrane transport of alkali and alkaline earth cations through graphene oxide membranes based on cation−π interactions, ACS Nano, 8 (2014) 850–859.
[47] W.S. Hummers Jr., R.E. Offeman, Preparation of graphitic oxide, J. Am. Chem. Soc., 80 (1958) 1339.
[48] Y. Wei, Y. Zhang, X. Gao, Y. Yuan, B. Su, C. Gao, Declining flux and narrowing nanochannels under wrinkles of compacted graphene oxide nanofiltration membranes, Carbon, 108 (2016) 568–575.
[49] C. Hontoria-Lucas, A.J. López-Peinado, J.D.D. López-González, M.L. Rojas-Cervantes, R.M. Martín-Aranda, Study of oxygen-containing groups in a series of graphite oxides: physical and chemical characterization, Carbon, 33 (1995) 1585–1592.
[50] S. Xia, M. Ni, T. Zhu, Y. Zhao, N. Li, Ultrathin graphene oxide nanosheet membranes with various d-spacing assembled using the pressure-assisted filtration method for removing natural organic matter, Desalination, 371 (2015) 78–87.
[51] J. Shen, M. Zhang, G. Liu, W. Jin, Facile tailoring of the two-dimensional graphene oxide channels for gas separation, RSC Adv., 6 (2016) 54281–54285.
[52] S.J. Chae, F. Güneş, K.K. Kim, E.S. Kim, G.H. Han, S.M. Kim, H.J. Shin, S.M. Yoon, J.Y. Choi, M.H. Park, Synthesis of large-area graphene layers on poly-nickel substrate by chemical vapor deposition: wrinkle formation, Adv. Mater., 21 (2009) 2328–2333.
[53] C. Vecchio, S. Sonde, C. Bongiorno, M. Rambach, R. Yakimova, V. Raineri, F. Giannazzo, Nanoscale structural characterization of epitaxial graphene grown on off-axis 4H-SiC (0001), Nanoscale Res. Lett., 6 (2011) 1–7.
[54] Y. Liu, C. Chen, Y. Li, X. Li, Q. Kong, M. Wang, Crumpled reduced graphene oxide by flame-induced reduction of graphite oxide for supercapacitive energy storage, J. Mater. Chem. A, 2 (2014) 5730–5737.
[55] X. Lin, X. Shen, Q. Zheng, N. Yousefi, L. Ye, Y. Mai, J. Kim, Fabrication of highly-aligned, conductive, and strong graphene papers using ultralarge graphene oxide sheets, ACS Nano, 6 (2012) 10708–10719.
[56] R.N. Wenzel, Resistance of solid surface to wetting by water, Ind. Eng. Chem., 28 (1936) 988–994.
[57] J. Muscatello, F. Jaeger, O.K. Matar, E.A. Müller, Optimizing water transport through graphene-based membranes: insights from nonequilibrium molecular dynamics, ACS Appl. Mater. Interfaces, 8 (2016) 12330–12336.
[58] D.D. Borges, C.F. Woellner, P.A. Autreto, D.S. Galvao, Water permeation through layered graphene-based membranes: a fully atomistic molecular dynamics investigation, arXiv Preprint, (2017) arXiv:1702.00250.
[59] J. Schaep, B. Van der Bruggen, C. Vandecasteele, D. Wilms, Influence of ion size and charge in nanofiltration, Sep. Purif. Technol., 14 (1998) 155–162.
[60] J. Peeters, J.P. Boom, M. Mulder, H. Strathmann, Retention measurements of nanofiltration membranes with electrolyte solutions, J. Membr. Sci., 145 (1998) 199–209.

Supplementary information

The ultrafiltration membranes were prepared by non-solvent induced phase inversion method. The component of casting solution was polysulfone (PSf) (18 wt.%), polyvinylpyrrolidone (PVP) (3 wt.%). PSf and PVP were dissolved in dimethylacetamide (DMAc) by continuous stirring for 4 h at 50°C. Then, the casting solution was kept overnight at room temperature until no air bubbles in the solution. The PSf solution was cast on a nonwoven polyester support layer by using a stainless steel knife. The membrane was then immersed in distilled water at 20°C. After primary phase inversion process, the membranes were kept in water for 24 h to remove the rest DMAc and PVP. The surface morphology and pores can be seen in SEM images (Fig. S1).

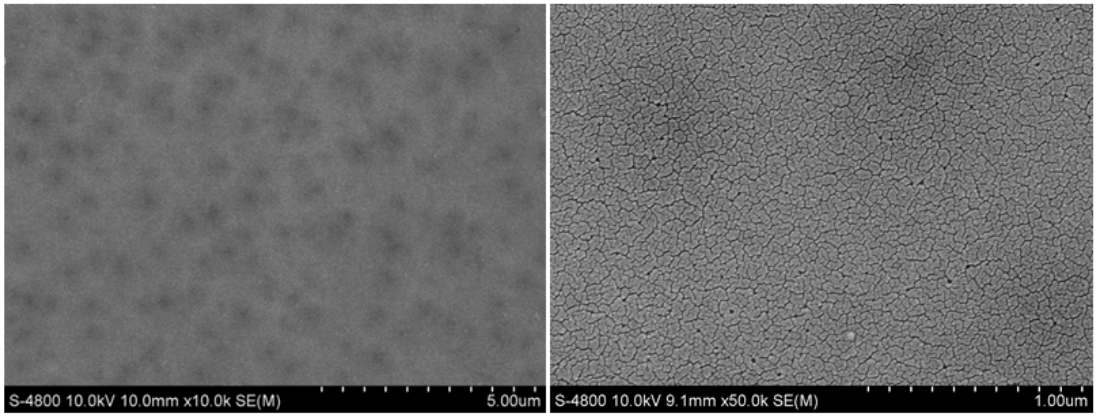

Fig. S1. SEM images of PSf membrane.